NASA/TM-20205001668

Baseline Optical Design for an Integrated Radio and Optical Communication System

Adam C. Wroblewski
Glenn Research Center, Cleveland, Ohio

January 2021

NASA STI Program . . . in Profile

Since its founding, NASA has been dedicated to the advancement of aeronautics and space science. The NASA Scientific and Technical Information (STI) Program plays a key part in helping NASA maintain this important role.

The NASA STI Program operates under the auspices of the Agency Chief Information Officer. It collects, organizes, provides for archiving, and disseminates NASA's STI. The NASA STI Program provides access to the NASA Technical Report Server—Registered (NTRS Reg) and NASA Technical Report Server—Public (NTRS) thus providing one of the largest collections of aeronautical and space science STI in the world. Results are published in both non-NASA channels and by NASA in the NASA STI Report Series, which includes the following report types:

- TECHNICAL PUBLICATION. Reports of completed research or a major significant phase of research that present the results of NASA programs and include extensive data or theoretical analysis. Includes compilations of significant scientific and technical data and information deemed to be of continuing reference value. NASA counter-part of peer-reviewed formal professional papers, but has less stringent limitations on manuscript length and extent of graphic presentations.

- TECHNICAL MEMORANDUM. Scientific and technical findings that are preliminary or of specialized interest, e.g., "quick-release" reports, working papers, and bibliographies that contain minimal annotation. Does not contain extensive analysis.

- CONTRACTOR REPORT. Scientific and technical findings by NASA-sponsored contractors and grantees.

- CONFERENCE PUBLICATION. Collected papers from scientific and technical conferences, symposia, seminars, or other meetings sponsored or co-sponsored by NASA.

- SPECIAL PUBLICATION. Scientific, technical, or historical information from NASA programs, projects, and missions, often concerned with subjects having substantial public interest.

- TECHNICAL TRANSLATION. English-language translations of foreign scientific and technical material pertinent to NASA's mission.

For more information about the NASA STI program, see the following:

- Access the NASA STI program home page at http://www.sti.nasa.gov

- E-mail your question to help@sti.nasa.gov

- Fax your question to the NASA STI Information Desk at 757-864-6500

- Telephone the NASA STI Information Desk at 757-864-9658

- Write to:
  NASA STI Program
  Mail Stop 148
  NASA Langley Research Center
  Hampton, VA 23681-2199

NASA/TM-20205001668

Baseline Optical Design for an Integrated Radio and Optical Communication System

Adam C. Wroblewski
Glenn Research Center, Cleveland, Ohio

National Aeronautics and
Space Administration

Glenn Research Center
Cleveland, Ohio 44135

January 2021

Acknowledgments

I wish to acknowledge the members of the iROC project team whose comments and advice were invaluable.

This report contains preliminary findings, subject to revision as analysis proceeds.

Level of Review: This material has been technically reviewed by technical management.

Available from

NASA STI Program
Mail Stop 148
NASA Langley Research Center
Hampton, VA 23681-2199

National Technical Information Service
5285 Port Royal Road
Springfield, VA 22161
703-605-6000

This report is available in electronic form at http://www.sti.nasa.gov/ and http://ntrs.nasa.gov/

Baseline Optical Design for an Integrated Radio and Optical Communication System

Adam C. Wroblewski
National Aeronautics and Space Administration
Glenn Research Center
Cleveland, Ohio 44135

Abstract

This document outlines the baseline optical design for an Integrated Radio and Optical communication (iROC) system, specifically the version labeled in-house as Lunar R1.2a. The version number corresponds to the particular design iteration, including major and minor changes that have been made throughout the design process. The catadioptric design is based on a reflective Cassegrain telescope configuration united with refractive tertiary components in order to approach a diffraction limited, laser beam expander communication transmitter. The configuration presented is intended to be used as an optical transmitter only. Optical design parameters, far-field beam propagations, optical component sensitivity studies, and design explorations are included to provide a high-level understanding of the beam expander's basic design requirements and optical performance.

Introduction

The optical reflector system is configured concentrically to a radio frequency (RF) parabolic primary reflector in order to provide a combined aperture system, which offers potentially lower mass and volume characteristics in comparison to joining two independent RF and optical terminals (Refs. 1 and 2). A generic concept is depicted in Figure 1.

This optical primary mirror design is governed by the RF primary's radius of curvature (ROC), 1.0 m, and the RF feedhorn's estimated aperture location at 0.5 m from the primary's vertex. This combined aperture relies upon the key feature that the optical aperture shares the same prescription to the RF primary reflector, which ensures that the optical primary contributes to the RF propagation. This document presents the baseline optical design, however, does not discuss additional engineering challenges that exist in the design of a concentrically configured integrated radio and optical transmitter system. Subsequent design challenges involve the implementation of fully coupled multiphysics analyses consisting of structural, thermal, optical performance (STOP) analyses together with RF propagation evaluations through the beam expander structure (Ref. 3).

Optical Design

The Cassegrain optical subsystem prescription is listed in Table 1, generated by an in-house analytical Cassegrain & Ritchey-Chrétien (RC) telescope design tool. This software suite is based on closed-form analytical prescription expressions and has been coded to provide a means for sweeping design parameters to provide system level evaluations of beam expander configurations, illustrated Figure 8, Figure 9, and Figure 10 (Ref. 4). The RC telescope offers the performance advantage of minimizing aberrations for non-zero field-angles and non-zero field-positions, however, this beam expander system is only intended for zero field-angle and zero field-position beam propagation. Given this mode of operation, both Cassegrain and RC beam expanders offer equivalent optical performance. From the optical fabrication, metrology and alignment perspective, the Cassegrain prescription is advantageous

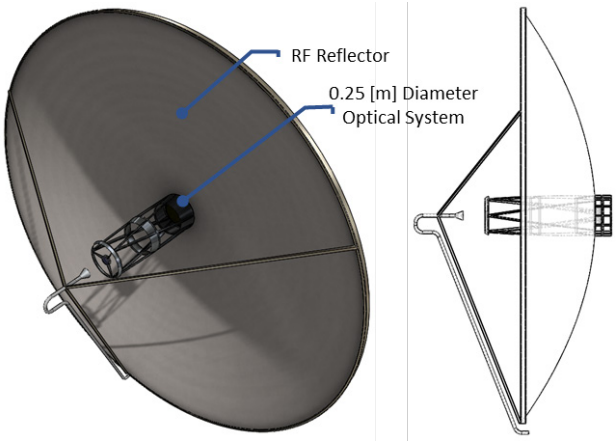

Figure 1.—Concentrically configured RF and optical system concept.

TABLE 1.—CASSEGRAIN OPTICAL SYSTEM PROPERTIES

***** General Solution Parameters *****	Value	Unit
Wavelength	1.55	µm
Primary Mirror OD	0.25	m
Primary Mirror ID	0.01	m
Primary Mirror Focal Length	0.5	m
Primary to Secondary Vertex to Vertex Distance	0.45	m
Back Focal Location Behind Primary Vertex	0.1	m
System F#	22	----
System Magnification	11	X
System Focal Length	5.5	----
Primary Reflector Surface Area	0.0492	m^2
Airy Disc Diameter	83.1808	µm
Full Focal Cone Angle	2.6006	deg
Obscuration Ratio (in Terms of Aperture OD)	0.1	D
***** Cassegrain Prescription Solution *****	--------	----
Primary Reflector Outer Diameter	0.25	m
Primary Reflector Radius of Curvature	1	m
Primary Reflector Conic Constant (CASS)	–1	----
Secondary Reflector Outer Diameter	0.025	m
Secondary Radius of Curvature (CASS)	0.11	m
Secondary Reflector Conic Constant (CASS)	–1.44	----
Spherical Aberration (Seidel Coeff)	0	----
Comatic Aberration (Seidel Coeff)	0.01653	----
Astigmatic Aberration (Seidel Coeff)	3.3388	----
***** Ritchey-Chrétien Prescription Solution *****	--------	----
Primary Reflector Outer Diameter	0.25	m
Primary Reflector Radius of Curvature	1	m
Primary Reflector Conic Constant (RC)	–1.0018	----
Secondary Reflector Outer Diameter	0.025	m
Secondary Radius of Curvature (RC)	0.11	m
Secondary Reflector Conic Constant (RC)	–1.4644	----
Aplanatic Sperical Aberration (Seidel Coeff)	–5.7896E-17	----
Aplanatic Comatic Aberration (Seidel Coeff)	–3.4694E-16	----
Aplanatic Astigmatic Aberration (Seidel Coeff)	3.4876	----

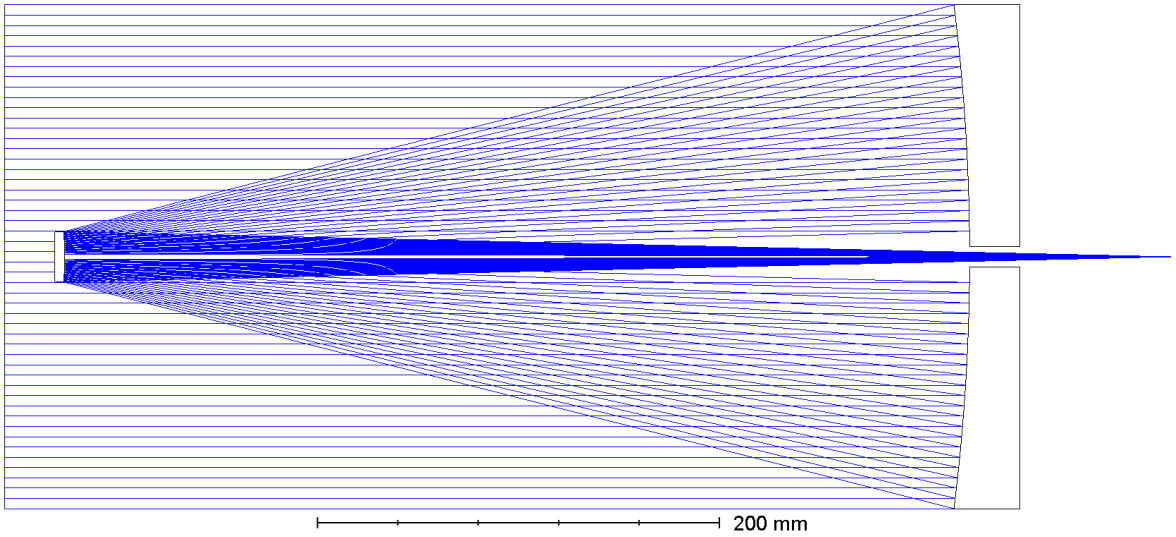

Figure 2.—Raytrace of the isolated Cassegrain optical system.

based on having a parabolic primary mirror, as opposed to the hyperbolic figure in an RC design. As a result of having an advantage in easier metrological operations and having equivalent optical performance to the RC, the beam expander design has adopted the Cassegrain prescription. For reference, assembly and alignment procedures have been developed for the proposed optical system (Ref. 5). An optical layout of the focal Cassegrain system is illustrated in Figure 2. For RF integration, the Cassegrain subsystem design has been bounded by a four constraints; a 0.25 m diameter optical primary mirror, a minimized secondary optic obscuration ratio, a matched optical/RF primary reflector radius of curvature (ROC), and a 0.1 m back-focal location. Based on these bounding criteria, the resulting telescope properties are computed.

The Cassegrain optical subsystem has been designed to illuminate the 0.25 m exit aperture with a 0.25 m diameter ($1/e^2$) Gaussian beam profile. The optical clipping loss associated has been identified to be approximately 23 percent, which includes aperture clipping, secondary reflector obscuration, and a three-spoke spider RF feedhorn support structure. The corresponding clipping mask is illustrated in Figure 3. In this design approach, the secondary reflector diameter is governed by the primary-to-secondary distance, where in this case, the secondary mirror vertex has been positioned 50 mm from the RF feedhorn. A proposed flight version of the secondary optical reflector would be fabricated from an RF transparent material, intended to minimize RF attenuation. The secondary reflector has been configured to produce a relatively low obscuration ratio of 0.1 D, where D is the 0.25 m aperture diameter. The optical spider support blockage has been assumed to have a 10 mm width, since the RF feedhorn struts are significantly larger than the optical secondary spider structure.

The left plot in Figure 4 illustrates the normalized aperture illumination at the aperture's exit plane. Based on the computed wavefront at the exit aperture illustrated in Figure 5, the resulting far field diffraction pattern is illustrated on the right plot in Figure 4. The far-field profile is valid at distances greater than the Rayleigh range, which for a 0.25 m diameter Gaussian beam is approximately 31.67 km. The far field diffraction pattern produces D4σ full beam divergences of 57.2 and 60.2 μRad in the X and Y axes, respectively. Note, that the D4σ beam-width definition is defined by the ISO Standard 11146 for beam property calculations (Ref. 6), which implements the second moment of intensity distribution. For ideal Gaussian beams, the D4σ method produces the same beam-width value as for the $1/e^2$ method, however, it can substantially deviate with other beam shapes. Note that, the full width beam divergence

based on the $1/e^2$ definition is approximately 11 µRad, and the –3 dB full width beam divergence is approximately 7 µRad. These beam divergence values can be used towards defining the magnitude of pointing accuracy needed from the stabilization, attitude determination, and pointing systems.

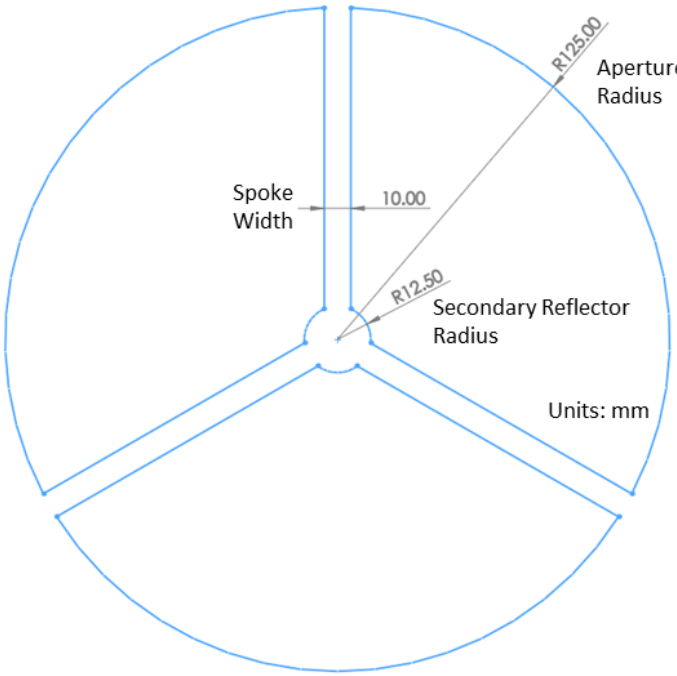

Figure 3.—Aperture clipping mask based on aperture diameter, secondary mirror, and 3-spoke RF feedhorn structure.

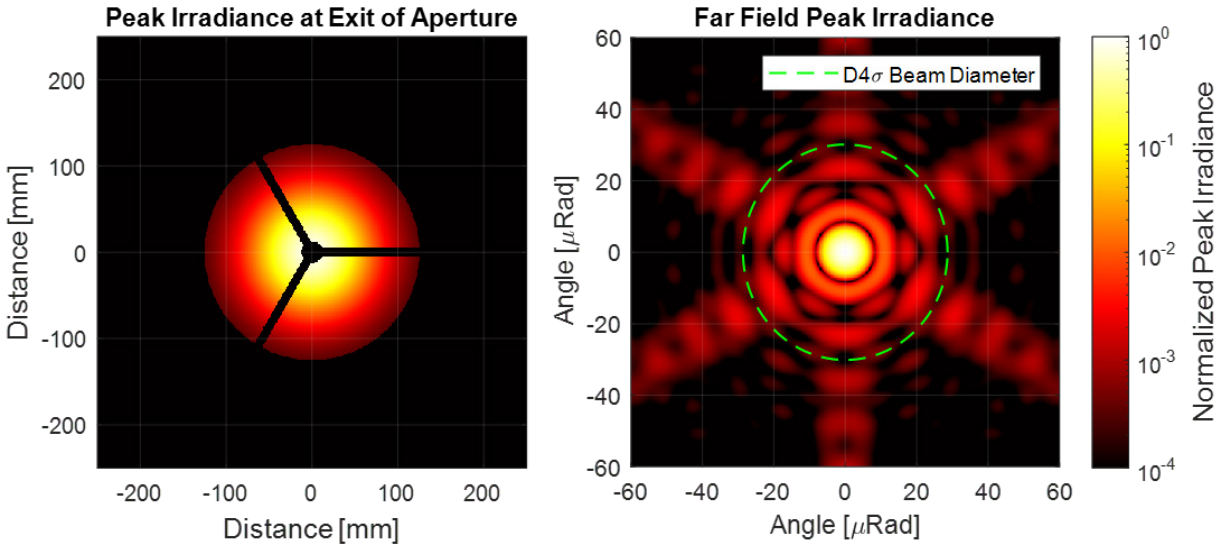

Figure 4.—Irradiance profile at aperture exit.

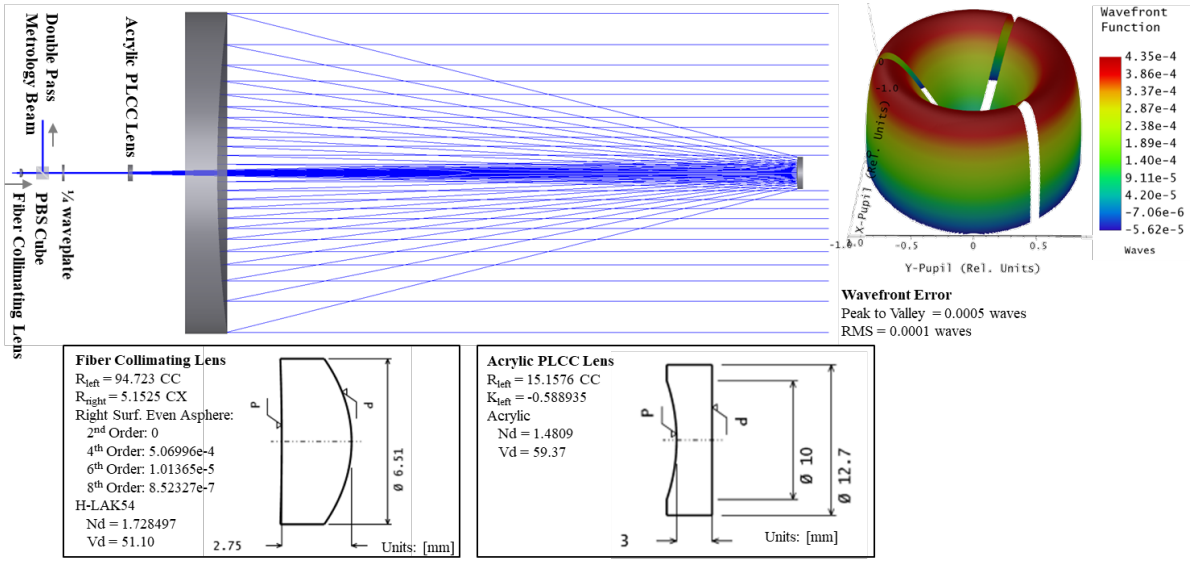

Figure 5.—Top left: Complete optical system with double pass metrology option. Top right: Computed wavefront error. Bottom: Tertiary lenses.

The free space optical path is initiated with single-mode laser propagation with wavelength 1550 nm from a polarization maintaining single-mode fiber aperture, with nominal properties consisting of mode field diameter MFD ≅ 10.5 μm and an effective numerical aperture N_{eff} ≅ 0.094. The fiber-coupled collimating asphere produces an approximate 1.45 mm $1/e^2$ diameter collimated beam, followed by a polarizing beamsplitter cube (PBS), 1/4 waveplate (QWP), and a custom plano-concave (PLCC) lens (located –65.6 mm behind the primary mirror vertex), as illustrated in the raytrace in Figure 5. The custom PLCC lens is made from acrylic, and has an aspheric surface that was optimized to contribute zero figure wavefront error to the optical system. The acrylic PLCC lens, and aluminum secondary and primary reflectors are to be fabricated in-house using a single point diamond turning (SPDT) lathe. Surface figure accuracy and finish quality directly from the SPDT lathe are considered sufficient for in-house prototyping purposes.

To reserve the option for future double-pass metrology activities, the laser irradiance is linearly polarized and configured to pass through the PBS cube and gets converted into circular polarization at the QWP. In the case where a double-pass metrology scheme may be implemented, the circularly polarized irradiance is reflected back into the beam expander by a >0.25 m flat mirror and passed back through the same QWP to convert the circular polarization back into linear polarization rotated 90° relative to the original polarization axis. With this polarization arrangement, the PBS directs irradiance to the secondary optical path where an instrument/detector may be located, with very little loss and minimal reverse propagation into the fiber optic laser source. A variety of optical detectors may be installed such as quadrant detectors for high speed beam stabilization measurements or a wavefront measurement camera for beam quality quantification.

A Gaussian beam launched into the Cassegrain beam expander is subject to a back-reflection from the central portion of the secondary mirror. The back-reflections prevent the utilization of any metrology detector packages in the tertiary optic assembly as previously described. Figure 6 illustrates the required blanking diameter on the secondary mirror, which was computed by reversing the ray trace and configuring the Cassegrain system as beam reducer, i.e., a telescope. This approach easily identifies the blanking diameter to be approximately 2.58 mm. Methods such as applying absorptive coatings or removal of the region can be used to mitigate this back-reflection effect.

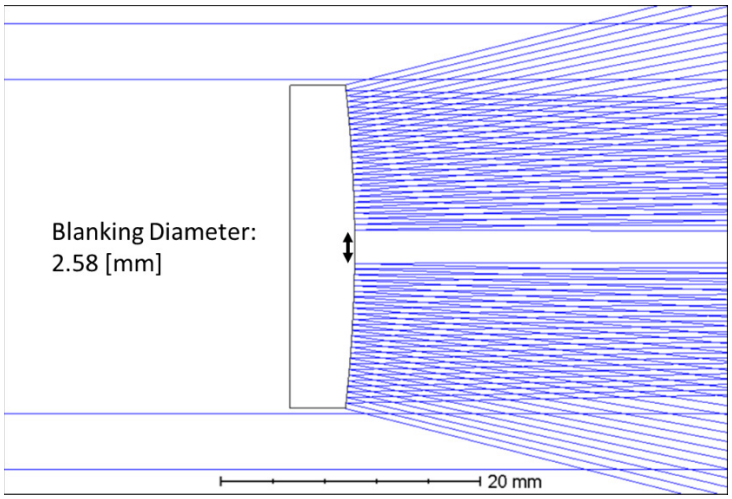

Figure 6.—Secondary mirror core blanking diameter.

Optical Sensitivities

Optical component sensitives of the fiber aperture, the fiber collimating lens, the PLCC lens, and the secondary mirror are examined to provide baseline assembly tolerances. In addition to optic location tolerancing, the fiber aperture and the secondary mirrors are of particular interest. The fiber optic is a candidate component for beam steering through application of lateral translation and the secondary reflector is an optical component that is highly susceptible to vibration due to its relatively remote location in the opto-mechanical structure.

The two main criteria for quantifying the beam's performance under the translational and rotational disturbances in the sensitivity studies are chief ray angle (CRA) and root mean square (RMS) wavefront error (WFE). The CRA relative to the optical axis is representative of the resulting pointing angle of the beam. The RMS wavefront represents the beam quality, i.e., how well the beam's far-field diffraction pattern remains intact compared to the best-case baseline form. Basic criteria for the beam's diffraction limit is typically considered greater than ~0.8 Strehl ratio, or less than ~0.0745 λ RMS wavefront error (Ref. 7). The bulk optical components have been swept in both rotation and translation DOFs to generate the subsequent sensitivity charts with the optical figure accuracy and surface finishes modeled as ideal. Positive and negative rotations about the X and Y axes produce identical results and are not duplicated. Rotation about the Z axis does not have an effect. Positive and negative translations in the X and Y directions produce identical results, however, positive and negative translations in the Z axis produce slightly different results and are listed. A basic assumption for upholding open-loop optical alignment has been to maintain a CRA within the 3 dB beam width, i.e., ± 3.5 μRad semi-angle, and diffraction limited beam performance, i.e., <0.075 λ RMS WFE. Note that implementation of closed-loop feedback control based on some variation of optical beam sampling/metrology can substantially relax the optical component positioning tolerances, which may be investigated in subsequent efforts.

Table 2 lists the sensitivity of the secondary reflector. Note that the point of rotation of the secondary during the displacements is located at the surface vertex. It can be observed that the CRA is substantially more sensitive to optical displacements than WFE, except in the Z translation case. One can infer that beam pointing error will be a dominant effect in the presence of small secondary optic displacements while the far-field diffraction pattern will remain relatively intact.

TABLE 2.—SECONDARY REFLECTOR SENSITIVITY

DOF	Input translation, mm	Input rotation, deg	CRA, μRad	WFE RMS, λ
ROT. ±X & ±Y	----------	0.000000000	0.000000000	0.000100000
	----------	0.000100000	0.349066000	0.000100000
	----------	0.001000000	3.490660000	0.000700000
	----------	0.010000000	34.906600000	0.006600000
	----------	0.100000000	349.064429203	0.066100000
	----------	1.000000000	3489.097126798	0.556700000
TRANS. ±X & ±Y	0.000000000	----------	0.000000000	0.000100000
	0.000100000	----------	0.182613878	0.000100000
	0.001000000	----------	1.826086419	0.000800000
	0.010000000	----------	18.260881644	0.007500000
	0.100000000	----------	182.608292844	0.075400000
	1.000000000	----------	1825.614796027	0.684900000
TRANS. Z	–1.000000000	----------	0.000000000	5.417000000
	–0.100000000	----------	0.000000000	0.542700000
	–0.010000000	----------	0.000000000	0.054300000
	–0.001000000	----------	0.000000000	0.005400000
	–0.000100000	----------	0.000000000	0.000600000
	0.000000000	----------	0.000000000	0.000100000
	0.000100000	----------	0.000000000	0.000500000
	0.001000000	----------	0.000000000	0.005400000
	0.010000000	----------	0.000000000	0.054300000
	0.100000000	----------	0.000000000	0.542900000
	1.000000000	----------	0.000000000	5.438400000

The translation of the fiber optic aperture is a candidate solution for beam steering or stabilization. Note that another common solution to steering/stabilization is the introduction of a fast steering mirror (FSM) into the optical path. Although an FSM is a reliable approach to beam steering, an effort has been made to minimize the number of components in the optical path as well as maintaining as much axial symmetry as possible. For this reason, the fiber positioner strategy has been a leading candidate for a beam steering/stabilization approach. In this case, the small lateral fiber aperture displacements listed in Table 3 provide a substantial amount of CRA with minimal effect on WFE. Small angular rotations of the fiber optic source induces negligible CRA or WFE.

The fiber collimator lens sensitivity is listed in Table 4, having a point of rotation on the vertex of the concave surface. Similarly, the PLCC lens sensitivity is listed in Table 5, having the point of rotation on the vertex of the concave surface. In both tables, one can observe that the CRA is more substantially affected than the WFE in presence of X, Y translations and rotations. The Z translation has no effect on the CRA but does impart WFE.

For the purpose of accelerating the in-house prototyping process, there is a variation to the baseline optical system. In this variation, the original wavelength of 1550 nm is substituted for a visible 633 nm wavelength along with an equivalent commercial off the shelf (COTS) visible wavelength coated fiber collimator lens and a COTS spherical PLCC lens (diameter: 12.7 mm, ROC: –12.86 mm, material: N-BK7). The location of the COTS PLCC lens is adjusted to a location of –71.52 mm behind the primary mirror vertex. The substitution of a spherical PLCC lens results in the predicted WFE of approximately 0.0254 λ RMS.

TABLE 3.—FIBER POSITION SENSITIVITY

DOF	Input translation, mm	Input rotation, deg	CRA, μRad	WFE RMS, λ
ROT. ±X & ±Y	----------	0.000000000	0.000000000	0.0001
	----------	0.000100000	0.000000000	0.0001
	----------	0.001000000	0.000017453	0.0001
	----------	0.010000000	0.000087266	0.0001
	----------	0.100000000	0.000890118	0.0001
	----------	1.000000000	0.008203047	0.0003
TRANS. ±X & ±Y	0.000000000	----------	0.000000000	0.0001
	0.000100000	----------	0.076881754	0.0001
	0.000500000	----------	0.384443674	0.0001
	0.001000000	----------	0.768904802	0.0001
	0.005000000	----------	3.844489103	0.0001
	0.010000000	----------	7.688925847	0.0001
	0.050000000	----------	38.43605967	0.0006
	0.100000000	----------	76.81862499	0.0008
TRANS. Z	–1.000000000	----------	0.000000000	0.2918
	–0.100000000	----------	0.000000000	0.0702
	–0.010000000	----------	0.000000000	0.0081
	–0.001000000	----------	0.000000000	0.0008
	–0.000100000	----------	0.000000000	0.0002
	0.000000000	----------	0.000000000	0.0001
	0.000100000	----------	0.000000000	0.0002
	0.001000000	----------	0.000000000	0.0008
	0.010000000	----------	0.000000000	0.0080
	0.100000000	----------	0.000000000	0.0678
	1.000000000	----------	0.000000000	0.4750

TABLE 4.—FIBER COLLIMATOR LENS SENSITIVITY

DOF	Input translation, mm	Input rotation, deg	CRA, μRad	WFE RMS, λ
ROT. ±X & ±Y	----------	0.000000	0.000000000	0.0001
	----------	0.000100	0.002268928	0.0001
	----------	0.001000	0.022619467	0.0001
	----------	0.010000	0.226264484	0.0001
	----------	0.100000	2.262679749	0.0001
	----------	1.000000	22.626116810	0.0005
TRANS. ±X & ±Y	0.000000000	----------	0.000000000	0.0001
	0.000100000	----------	0.076881754	0.0001
	0.000500000	----------	0.384443674	0.0001
	0.001000000	----------	0.768904802	0.0001
	0.005000000	----------	3.844489103	0.0001
	0.010000000	----------	7.688908393	0.0001
	0.050000000	----------	38.43365111	0.0007
	0.100000000	----------	76.79949618	N/A
TRANS. Z	–1.00000000	----------	0.000000000	0.2918
	–0.10000000	----------	0.000000000	0.0702
	–0.01000000	----------	0.000000000	0.0081
	–0.00100000	----------	0.000000000	0.0008
	–0.00010000	----------	0.000000000	0.0002
	0.000000000	----------	0.000000000	0.0001
	0.000100000	----------	0.000000000	0.0002
	0.001000000	----------	0.000000000	0.0008
	0.010000000	----------	0.000000000	0.0080
	0.100000000	----------	0.000000000	0.0678
	1.000000000	----------	0.000000000	0.4750

TABLE 5.—PLCC LENS SENSITIVITY

DOF	Input translation, mm	Input rotation, deg	CRA, μRad	WFE RMS, λ
ROT. ±X & ±Y	----------	0.000000	0.000000000	0.0001
	----------	0.000100	0.000296706	0.0001
	----------	0.001000	0.003036873	0.0001
	----------	0.010000	0.030368729	0.0001
	----------	0.100000	0.303704743	0.0001
	----------	1.000000	3.037326684	0.0006
TRANS. ±X & ±Y	0.000000000	----------	0.000000000	0.0001
	0.000100000	----------	0.018186331	0.0001
	0.000500000	----------	0.090914201	0.0001
	0.001000000	----------	0.181810948	0.0001
	0.005000000	----------	0.909089647	0.0001
	0.010000000	----------	1.818179295	0.0001
	0.050000000	----------	9.090879022	0.0001
	0.100000000	----------	18.18165332	0.0001
TRANS. Z	–1.000000000	----------	0.000000000	0.0447
	–0.100000000	----------	0.000000000	0.0045
	–0.010000000	----------	0.000000000	0.0005
	–0.001000000	----------	0.000000000	0.0001
	–0.000100000	----------	0.000000000	0.0001
	0.000000000	----------	0.000000000	0.0001
	0.000100000	----------	0.000000000	0.0001
	0.001000000	----------	0.000000000	0.0001
	0.010000000	----------	0.000000000	0.0050
	0.100000000	----------	0.000000000	0.0045
	1.000000000	----------	0.000000000	0.0456

Design Exploration

Additional examinations of the reflective optical prescriptions provide insights into the spherical departure of the primary mirror and secondary mirror of the proposed baseline design. The plots in Figure 7 illustrate that the magnitude of departure from a spherical surface for both Cassegrain and RC configuration are nearly identical for this long focal length beam expander. The spherical departure is shown in both units of microns and wavelengths and can be useful for planning subsequent interferometric testing operations.

Figure 8, Figure 9, and Figure 10 illustrate sweeps of the primary-to-secondary mirror separation distance of the Cassegrain system with resulting dependent Cassegrain and RC properties on the Y-axis. Parameter sweeps are essential for design exploration and as well as system level considerations early in the design process. The design exploration studies were generated by an in-house telescope design tool, specifically coded to sweep design variables and examine the effects of other telescope properties. The independent variable that was swept in this design exploration is the primary and secondary mirrors vertex to vertex distance, since telescope physical length was one of the key features of interest in the beam expander design objectives. The fixed parameters are the design wavelength, 1.55 um, the primary mirror diameter, 0.25 m, and the primary mirror focal length, 0.5 m. For instance, Figure 8 illustrates that as the secondary mirror is placed closer to the RF feedhorn (located at 0.5 m from the primary mirror's vertex), the secondary mirror diameter is minimized, which aligns with the objective of minimizing the obscuration ratio. However, a reasonable standoff distance from the RF feedhorn is necessary, which was selected to be approximately 50 mm. This resulted in a proposed secondary mirror diameter of 25 mm, which also favorably reduces the optical cone angle as well as the secondary's ROC.

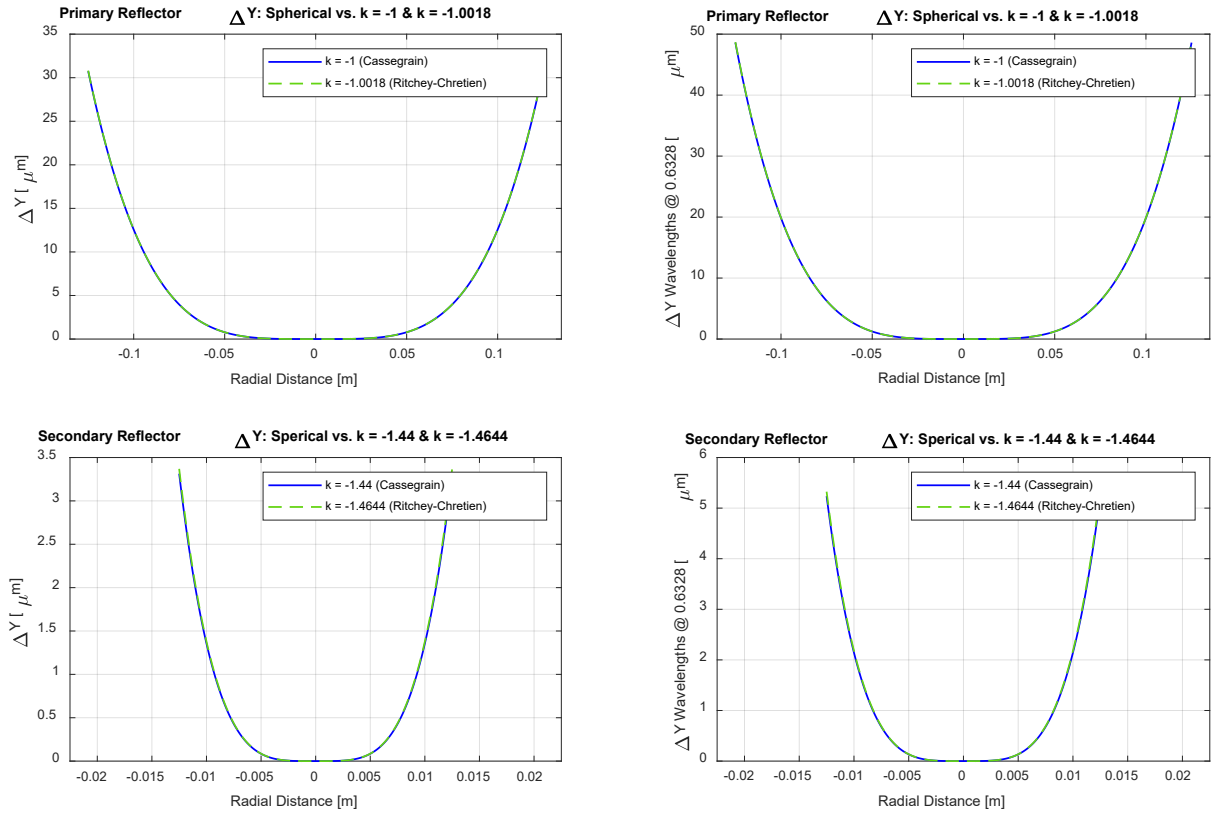

Figure 7.—Primary and secondary mirror spherical departures.

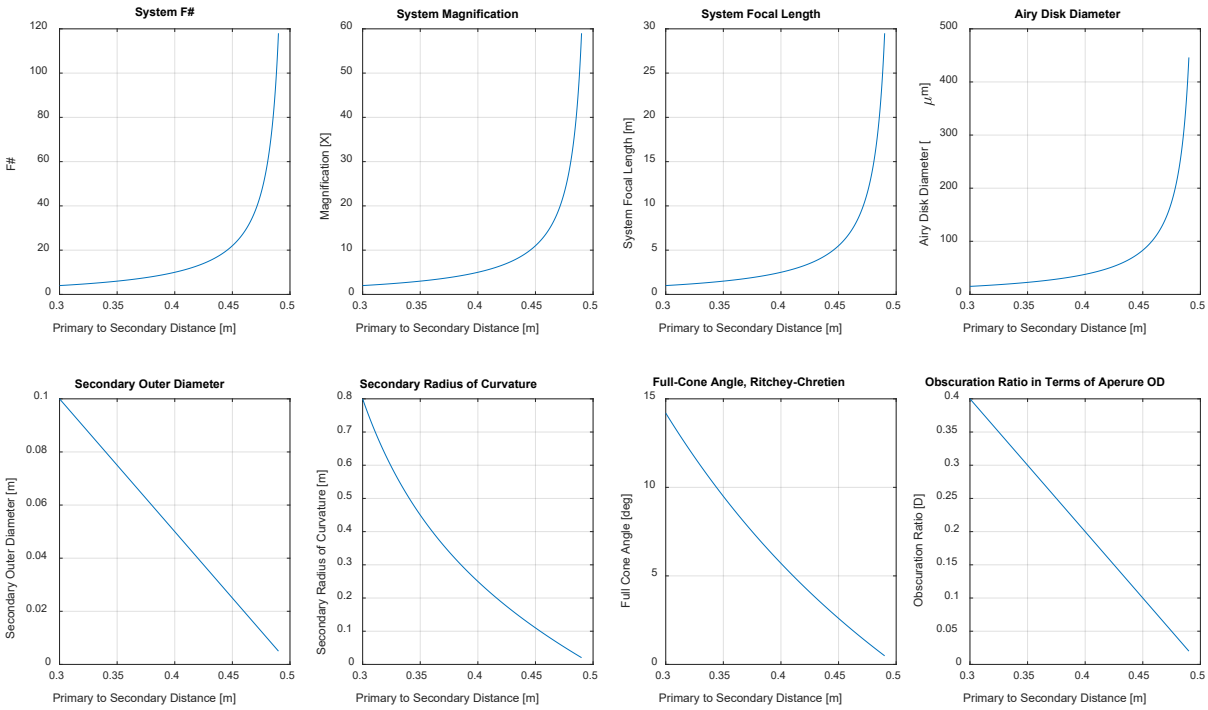

Figure 8.—A set of beam expander parameters as a function of length.

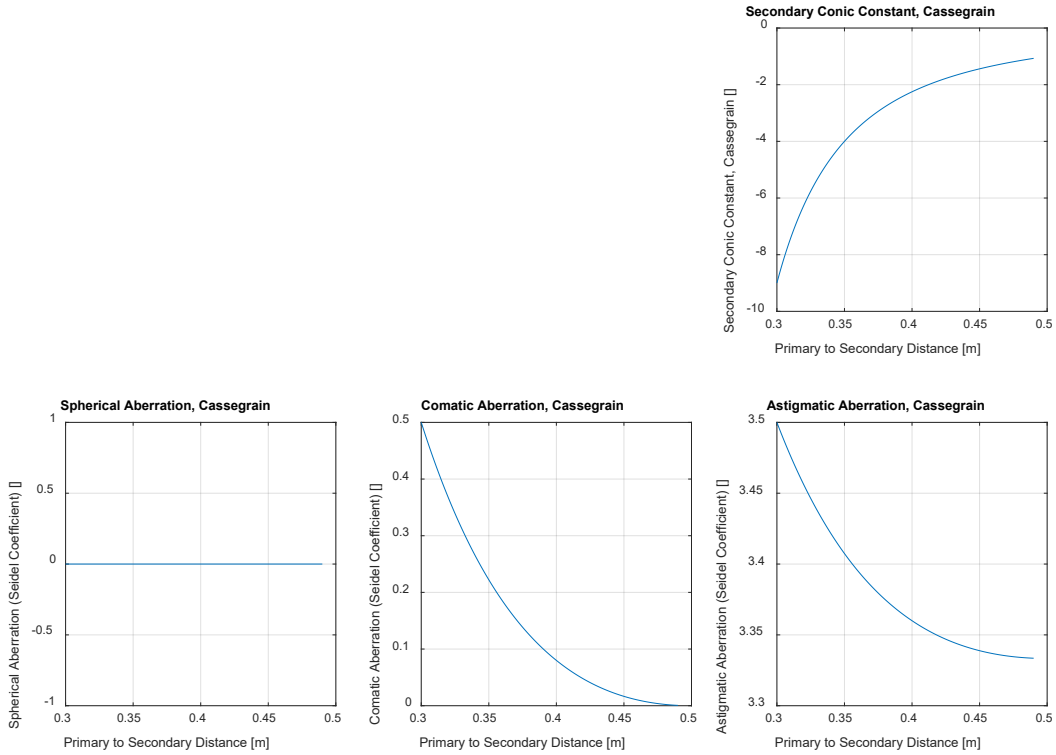

Figure 9.—A set of Cassegrain beam expander design parameters as a function of length.

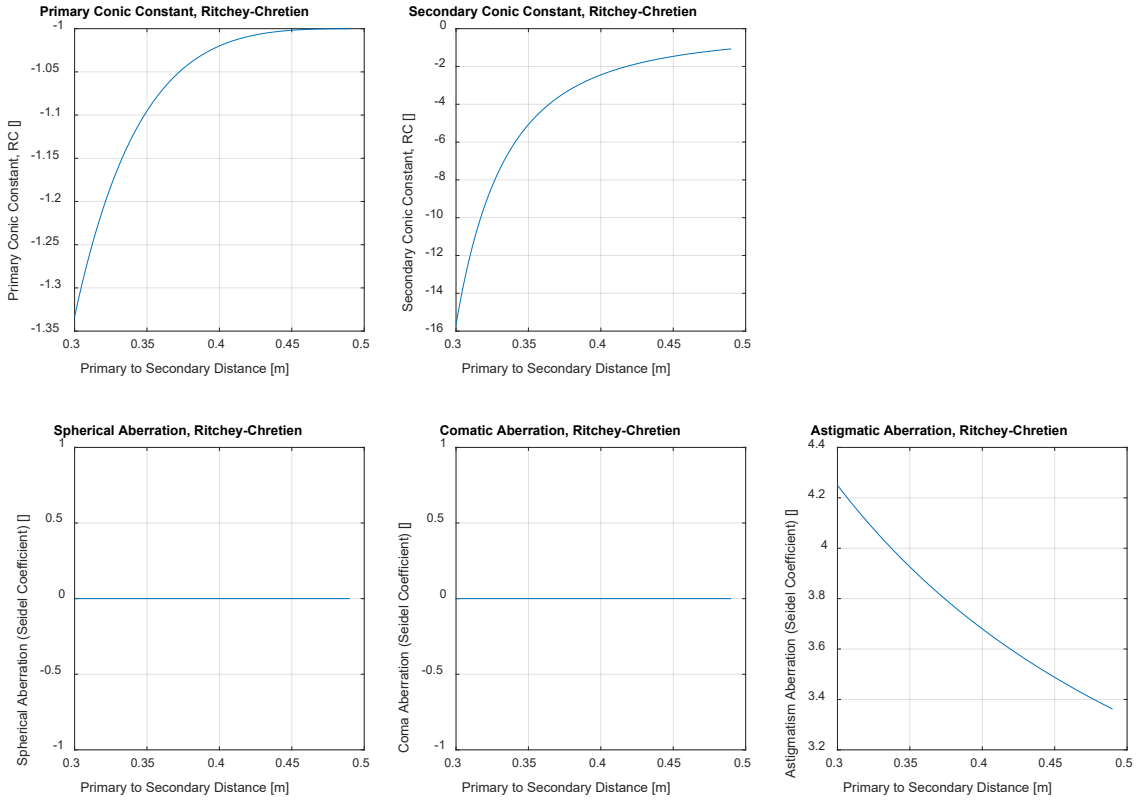

Figure 10.—A set of RC beam expander design parameters as a function of length.

Conclusion

A baseline optical design has been presented along with relevant optical design parameters, a far field beam propagation analysis, optical component sensitivity studies, and design explorations towards the objective of fabricating an in-house laser communication beam expander system. This examination provides a reference point for developing optical design concepts for use in subsequent co-boresighted optical and RF development efforts. Noteworthy steps forward to advance the optical system technology are to develop optimal opto-mechanical structural models for STOP evaluations, develop a closed-loop feedback-controlled optical alignment strategy, and continue development of an RF transparent beam expander structure.

References

1. Raible, D.E., Romanofky, R.R., Budinger, J.M., Nappier, J.M., Hylton, A.G., Swank, A.J., Nerone, A.L., "On the Physical Realizability of Hybrid RF and Optical Communications Platforms for Deep Space Applications," 32nd AIAA International Communications Satellite Systems Conference, San Diego, CA., August 2014.
2. Raible, D., Hylton, A.G., "Integrated RF/Optical Interplanetary Networking Preliminary Explorations and Empirical Results," 30th AIAA International Communications Satellite System Conference (ICSSC). https://doi.org/10.2514/6.2012-15126.
3. Wroblewski, A.C., "Hybrid Communication System Including A Mounting Structure For An Optical Element," U.S. Patent 10,673,146 B1 Jun. 2, 2020.
4. R.N. Wilson, "Reflecting Telescope Optics I: Basic Design Theory and its Historical Development," Springer Science & Business Media, Mar 9, 2013.
5. Greenberg, P.S., "Integrated Radio and Optical Communications (iROC) Primary, Secondary, and Tertiary Optics Alignment Procedure," NASA Technical Memorandum 20200004351, July 1, 2020.
6. *Zemax OpticStudio 20.3 User Manual.* September 2020.
7. V.N. Mahajan, "Aberration Theory Made Simple, Second Edition", 2011, https://doi.org/10.1117/3.903924.